

Arsenic evolution as a tool for understanding formation of pyritic gold ores

Yanlu Xing¹, Joël Brugger^{1,*}, Andrew Tomkins¹, Yuri Shvarov²

1. School of Earth, Atmosphere and Environment, Monash University, Clayton, VIC 3800, Australia

2. Lomonosov Moscow State University, Moscow, Russia

* Corresponding author. joel.brugger@monash.edu

Description of the model and fundamental assumptions

(i) In the absence of a reliable experimentally derived phase diagram for the $\text{FeAs}_2\text{-FeS}_2$ system, we use the phase diagram derived by Reich and Becker (2006) based on first-principle quantum mechanical techniques. This has the advantage of providing a self-consistent thermodynamic framework for As in pyrite/marcasite, which has a clear crystal chemical foundation, and appears to qualitatively fit with the existing experimental and natural observations (see discussion in Reich and Becker 2006).

(ii) Our model accounts only for the substitution of As on the S site of pyrite/marcasite, which is the main form of As in pyrite/marcasite in nature. Under some conditions, As acts as a cation, and replaces Fe^{2+} in pyrite/marcasite (e.g., epithermal deposits, Deditius et al., 2008; coal, Etschmann et al., 2017). Experiments suggest that in some cases at least, this reflects reaction mechanism rather than equilibrium (Qian et al. 2013), and our model does not attempt to reproduce this substitution.

(iii) To model the FeS_2 - FeAs_2 binary, we consider three phases: FeS_2 (pyrite/marcasite), FeAsS (arsenopyrite) and FeAs_2 (löllingite). Löllingite is assumed to be pure and stoichiometric; this reflects the absence of data on the composition of natural löllingite, in addition to the limited S solubility in this mineral. FeS_2 (pyrite/marcasite) is described as a solid solution ($\text{Fe}(\text{S,As})_2$) between marcasite and a fictional löllingite. The fictional löllingite was defined such as $\Delta G_{Lo}^{fic} = \Delta G_{Lo} + 10\text{kJ/mole}$. This insures that löllingite is the stable mineral on the As-rich side of the diagram. Arsenopyrite was modelled as a solid solution between the fictional end-members low-As arsenopyrite (AspLow, $\text{FeS}_{1.2}\text{As}_{0.8}$) and high-As arsenopyrite (AspHigh, $\text{FeS}_{0.8}\text{As}_{1.2}$). Figure DR1 shows that the Gibbs free energy of formation from the elements ($\Delta_f G^0$) at each P-T for these endmembers was assumed to represent ideal mixing between the isomorphous marcasite and löllingite.

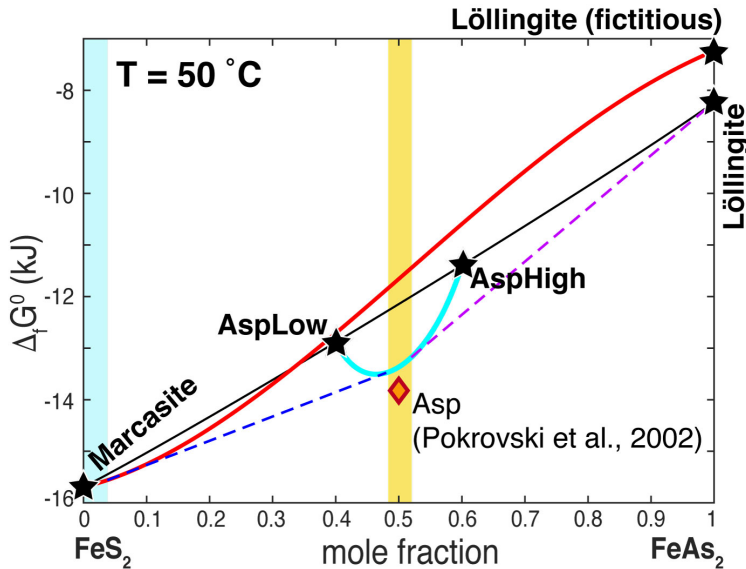


Figure DR1. Example Gibbs free energy diagram for the model of the FeS_2 - FeAs_2 joint developed in this study (50 °C). The solid red line is the Gibbs free energy of formation from the elements of the pyrite solid-solution, and the solid magenta line that of arsenopyrite solid-solution. The thin solid black line is the ideal mixing between marcasite and löllingite. The end-members used in the model are labelled in bold font. The end-member stoichiometric arsenopyrite proposed by Pokrovski et al. (2002) is also shown for reference. Dashed lines are the tangents to the Gibbs free energy lines, and colored fields the resulting extends of the compositions of the pyrite/marcasite and arsenopyrite solid solutions.

Non-ideality and model fitting

Non-ideal contributions need to be incorporated for realistic modeling of the FeS₂-FeAs₂ binary (Reich and Becker, 2006). A model for real solution is usually defined using the specific excess Gibbs free energy of mixing, expressed through mole fractions of its components. For binary solutions this function is commonly expressed as

$$\overline{G}_{ex} = x_1 x_2 \alpha_{12}, \quad (1)$$

where α_{12} is a function of the mole fractions x_1 and x_2 of its components. As α_{12} is a rather arbitrary function, it is multiplied by $x_1 x_2$ to satisfy the condition $\overline{G}_{ex} = 0$ at both ends of the interval $[0, 1]$, which correspond to pure components. The type of α_{12} function is often chosen for reasons of convenience and simplicity. Special cases include $\alpha_{12} = 0$ for ideal mixture; $\alpha_{12} = W$ for regular solutions; and $\alpha_{12} = W_1 x_1 + W_2 x_2$ for subregular solutions. Here we use a virial series known as the Redlich-Kister (or Guggenheim) model, where

$$\alpha_{12} = A_0 + A_1(x_1 - x_2) + A_2(x_1 - x_2)^2 + \dots \quad (2)$$

This form is convenient because it is consistent with the listed special cases. For the Redlich-Kister model adopted in HCh (Shvarov, 1999; Shvarov and Bastrakov 1999; Shvarov 2008):

$$\alpha_{ij} = A_{ij}^0 + A_{ij}^1(x_i - x_j) + A_{ij}^2(x_i - x_j)^2 \quad (3)$$

The constants A_{ij}^0 , A_{ij}^1 and A_{ij}^2 (the superscripts are an index, not a power) depend on temperature (T , Kelvin) and pressure (P , bar) only:

$$A_{ij}^k = A_{ij}^k + c_{ijT}^k T + c_{ijP}^k P \quad (4)$$

In order to retrieve A_{ij}^j parameters for pyrite/marcasite and arsenopyrite, we used non-linear least-square to minimize the difference between the phase boundaries derived from *first-principle* calculations by Reich and Becker (2006) and those from the thermodynamic model. A further constrain was added that minimizes the difference between the $G(P, T)$ of the stoichiometric arsenopyrite from the model and that provided by Pokrovski et al. (2002) (Figure DR1). For the final model, we neglected P-dependence of the model (no data available). We found out that FeS₂(ss) can be accurately modeled using the T-independent A_{ij}^j parameters. In contrast, the accuracy of the modeling of FeAsS(ss) improved significantly with the addition of the three parameters modeling the T-dependence, and the

final fit was conducted using a total of nine free parameters. Model parameters are given in [Tables DR1 and DR2](#).

Table DR1. Selected thermodynamic properties

	Löllingite	Pyrite	Marcasite	Pyrrhotite	Arsenopyrite	AspLow	AspHigh
Formula:	FeAs ₂	FeS ₂	FeS ₂	Fe _{0.875} S	FeAsS	FeAs _{0.8} S _{1.2}	FeAs _{1.2} S _{0.8}
$\Delta_f G_{298}^0$ [J/mol]	-80230	-160218	-155465	-98900	-136450	-132032	-116989
S_{298}^0 [J.mol ⁻¹ .K ⁻¹]	80.100	52.928	53.900	60.700	68.500	70.334	75.721
V_{298}^0 [J.bar ⁻¹]	2.7440	2.3940	2.4580	1.7490	2.6270	2.5724	2.6296
Cp parameters							
x T ⁰	76.69	74.80992	72.512	37.7276	75.51	84.3493	74.9135
x T	3.10•10 ⁻³	5.52288•10 ⁻³	8.991•10 ⁻³	2.47524•10 ⁻²	4.78•10 ⁻³	-6.48516•10 ⁻³	5.4564•10 ⁻³
x T ⁻²	-6.03•10 ⁻⁵	-	-1.1345•10 ⁻⁶		7.543•10 ⁻⁵	-1.74158•10 ⁻⁶	-8.156•10 ⁻⁵
		1.27612•10 ⁻⁶					
x T ^{-0.5}							
x T ²				5.382440•10 ⁻⁵			
Reference:	Perfetti et al., 2008	SUPCRT95	IVTANTERMO	Robie and Hemingway, 1995	Pokrovski et al., 2002	This study	This study

Table DR2. Redlich-Kister parameters for the arsenopyrite and pyrite/marcasite solid solutions

	i	j	A_{ij}^0	A_{ij}^1	A_{ij}^2
Arsenopyrite (ss)	FeAs _{0.8} S _{1.2}	FeAs _{1.2} S _{0.8}	-36734.9	-9703.4	18752.7
T			12.50	26.00	-62.60
P			0	0	0
Pyrite/ marcasite(ss)	Marcasite	Fictional löllingite	-734.3	-44254.1	711.1
T			0	0	0
P			0	0	0

Modelling of As solubility in pyrite/marcasite and arsenopyrite

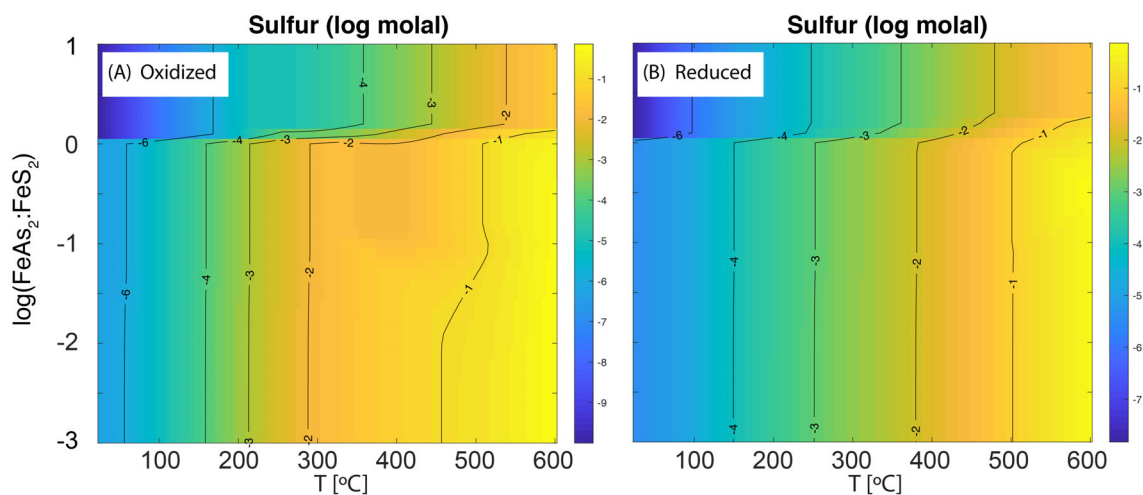


Figure DR2. Solubility of sulfur as a function of temperature and As:S ratio in oxidized fluids (A) and reduced fluids (B).

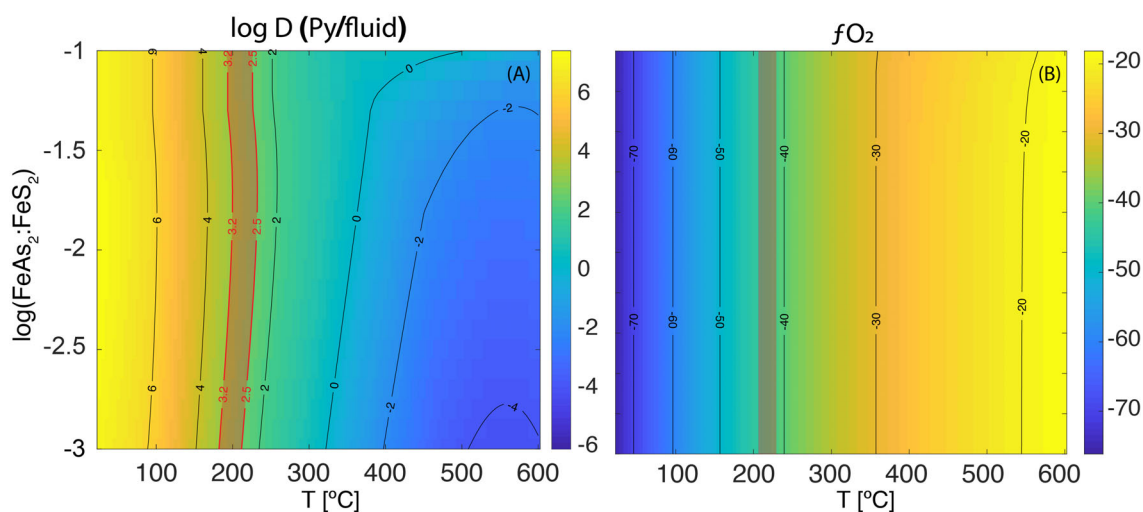


Figure DR3. Calculated partitioning coefficients of arsenic between pyrite and solution (A), and the map of fO_2 (B) for the oxidized system. (A) Shaded area indicates the value range of partitioning coefficients ($\log D_{\text{py/fluid}}$) for natural and experimental data from Kusebauch et al. (2018). (B) Shaded area indicates the fO_2 range for the experimental data of Kusebauch et al. (2018). Partitioning coefficients from ore deposits are in the range of 300-500 (Kusebauch et al., 2018; in gray on the diagrams), which fits with the predictions of the model. The data are drawn as grey isolines on Fig. 2C and 2D.

Modelling of multi-stage fluids alteration of pyritic ores

The starting composition of the modeled fluid and rocks are shown in [Table DR3](#). We used a basalt as the buffering rock of the ore fluids. The bulk composition of the basalt was adopted from the Fe-rich basalt presented by Phillips and Evans (2004), which reflects the rock units in the Eastern Goldfields of Australia. The starting fluid was first equilibrated with the basalt at a fluid/rock ratio of 1:1. The equilibrated fluid was then extracted and allowed to react with the low-As pyritic ore, using the step-flow-reactor model in HCh. Various batches of fresh fluid (waves in HCh terminology) were sequentially reacted to simulate increasing fluid:rock ratio.

Table DR3. Starting composition of the fluid and rocks used in the modeling

	Initial fluid	Basalt	Pyritic ore	Units
H ₂ O	1	0		kg
SiO ₂		587		g
Al ₂ O ₃		181		g
FeO		116		g
MgO		87		g
K ₂ O		6		g
Au		1.0•10 ⁻⁴		g
FeS ₂		1	495	g
FeAs ₂		0	4.95	g
CaO		23		g
As(OH) ₃	1.33E-03			mol
CO ₂	5.556			mol

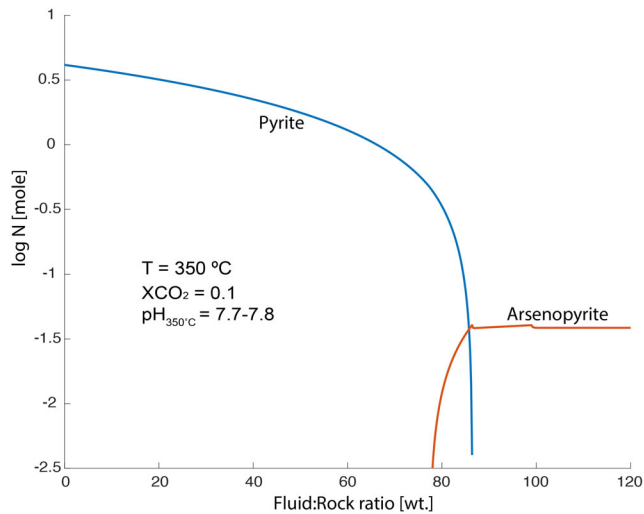


Figure DR4. Total amount of pyrite and arsenopyrite in the pyritic ores with changing fluid/rock ratio.

References

- Gurvich, L.V., IVTANTERMO-Thermodynamic Properties Database, Vestn. Akad. Nauk SSSR, 1983, no. 3, p. 54.
- Deditius, A.P. et al., 2008. A proposed new type of arsenian pyrite: Composition, nanostructure and geological significance. *Geochimica Et Cosmochimica Acta*, 72(12): 2919-2933.
- Etschmann, B. et al., 2017. Enrichment of germanium and associated arsenic and tungsten in coal and roll-front uranium deposits. *Chemical Geology*, 463: 29-49.
- Kusebauch, C., Oelze, M., Gleeson, S., 2018. Partitioning of arsenic between hydrothermal fluid and pyrite during experimental siderite replacement. *Chemical Geology*, In press.
- Perfetti, E., Pokrovski, G.S., Ballerat-Busserolles, K., Majer, V., Gibert, F., 2008. Densities and heat capacities of aqueous arsenious and arsenic acid solutions to 350 °C and 300 bar, and revised thermodynamic properties of, and iron sulfarsenide minerals. *Geochimica et Cosmochimica Acta*, 72: 713-731.
- Phillips, G.N., Evans, K.A., 2004. Role of CO₂ in the formation of gold deposits. *Nature*, 429(6994): 860-863.
- Pokrovski, G.S., Kara, S., Roux, J., 2002. Stability and solubility of arsenopyrite, FeAsS, in crustal fluids. *Geochimica Et Cosmochimica Acta*, 66(13): 2361-2378.
- Qian, G., Brugger, J., Testemale, D., Skinner, W., Pring, A., 2013. Formation of As(II)-pyrite during experimental replacement of magnetite under hydrothermal conditions. *Geochimica et Cosmochimica Acta*, 100: 1-10.
- Reich, M., Becker, U., 2006. First-principles calculations of the thermodynamic mixing properties of arsenic incorporation into pyrite and marcasite. *Chemical Geology*, 225(3-4): 278-290.

- Robie, R., Hemingway, B., 1995. Thermodynamic properties of minerals and related substances at 298.15 K and 1 bar (105 Pascals) pressure and higher temperatures. U.S. Geological Survey Bulletin, 2131.
- Shvarov, Y., 1999, Algorithmization of the Numeric Equilibrium Modeling of Dynamic Geochemical Processes: *Geochemistry International*, v. 37, no. 6, p. 571-576.
- Shvarov, Y., and Bastrakov, E., 1999, HCh: a software package for geochemical modelling. User's guide.
- Shvarov, Y., 2008, HCh: New potentialities for the thermodynamic simulation of geochemical systems offered by windows. *Geochemistry International*, v. 46, p. 834-839.